GA–A21904
CONF-941101--8

NONDIMENSIONAL TRANSPORT SCALING IN DIII–D: BOHM VERSUS GYRO-BOHM RESOLVED

by

C.C. PETTY, T.C. LUCE, K.H. BURRELL, S.C. CHIU, J.S. deGRASSIE, C.B. FOREST, P. GOHIL, C.M. GREENFIELD, R.J. GROEBNER, R.W. HARVEY, R.I. PINSKER, R. PRATER, R.E. WALTZ, R.A. JAMES,* and D. WRÒBLEWSKI*

This is a preprint of an invited paper presented at the 1994 American Physical Society Division of Plasma Physics Meeting, November 7–11, 1994, Minneapolis, Minnesota, and to be printed in the *Proceedings.*

Work supported by
U.S. Department of Energy under Contracts
DE–AC03–89ER51114 and W–7405–ENG–48

*Lawrence Livermore National Laboratory

GENERAL ATOMICS PROJECT 3466
FEBRUARY 1995

GENERAL ATOMICS

DISCLAIMER

Nondimensional transport scaling in DIII–D: Bohm versus gyro-Bohm resolved*

C.C. PETTY,† T.C. LUCE, K.H. BURRELL, S.C. CHIU, J.S. deGRASSIE, C.B. FOREST, P. GOHIL, C.M. GREENFIELD, R.J. GROEBNER, R.W. HARVEY, R.I. PINSKER, R. PRATER, and R.E. WALTZ

General Atomics
San Diego, California 92186-9784, U.S.A.

R.A. JAMES and D. WRÒBLEWSKI[a)]

Lawrence Livermore National Laboratory
Livermore, California 94550, U.S.A.

Abstract

The scaling of cross-field heat transport with relative gyroradius ρ_* was measured in low (L) and high (H) mode tokamak plasmas using the technique of dimensionally similar discharges. The relative gyroradius scalings of the electron and ion thermal diffusivities were determined separately using a two-fluid transport analysis. For L–mode plasmas, the electron diffusivity scaled as $\chi_e \propto \chi_B \rho_*^{1.1\pm0.3}$ (gyro-Bohm-like) while the ion diffusivity scaled as $\chi_i \propto \chi_B \rho_*^{-0.5\pm0.3}$ (worse than Bohm-like). The results were independent of the method of auxiliary heating (radiofrequency or neutral beam). Since the electron and ion fluids had different gyroradius scalings, the effective diffusivity and global confinement time scalings were found to vary from gyro-Bohm-like to Bohm-like depending upon whether the electron or ion channel dominated the heat flux. This last property can explain the previously disparate results with dimensionally similar discharges on different fusion experiments that have been published. Experiments in H–mode were also done with the expected values of beta, collisionality, safety factor, and plasma shape for thermonuclear ignition experiments. For these dimensionally similar discharges, both the electron and ion diffusivities scaled gyro-Bohm-like, $\chi_e, \chi_i \propto \chi_B \rho_*$, as did the global thermal confinement time. This leads to a very favorable prediction for the confinement time of future ignition devices.

---

*Paper 3IB3, Bull. Am. Phys. Soc. **39**, 1577 (1994).

†Invited speaker.

[a)]Present address: Maxwell Laboratories, San Diego, California.

CONTENTS

Figures

Tables

I. INTRODUCTION

Although it is widely believed that some form of plasma turbulence is responsible for the anomalous cross-field diffusion of heat in tokamaks and stellarators, the specific nature is still unknown despite much experimental effort. Historically, anomalous heat transport has been studied by systematically varying the engineering parameters such as the plasma current I, magnetic field strength B, plasma density n, and heating power $P_{\rm tot}$. Recently there has been a growing interest in measuring the scaling of confinement with the nondimensional parameters (for comparison with theoretical scalings[1]) such as safety factor $q \sim Ba/I$, beta $\beta \sim nT/B^2$, collisionality $\nu_* \sim qna/T^2$, and relative gyroradius $\rho_* = r_{\rm L}/a$ (in these relations, T is the plasma temperature, a is the plasma minor radius, and $r_{\rm L}$ is the Larmor radius). Plasmas which have identical values for all nondimensional parameters of interest except ρ_* are referred to as being "dimensionally similar." Of particular interest is the scaling of anomalous heat transport with ρ_*, since the confinement results of existing fusion experiments can be scaled to ignition devices of larger size and magnetic field by keeping all the nondimensional parameters fixed except for the relative gyroradius.[1]

A basic assumption of nondimensional scaling experiments is that transport is dependent only upon local quantities. Thus, following the scale invariance approach to confinement scaling,[2,3] the thermal diffusivity χ can be written as

$$\frac{\chi}{\chi_{\rm B}} = \rho_*^{x_\rho} F(q, \beta, \nu_*, T_{\rm e}/T_{\rm i}, \alpha_{\rm n}, \alpha_{\rm T}, \cdots) \quad , \tag{1}$$

where $\chi_{\rm B} = cT_{\rm e}/eB$ is the Bohm diffusion coefficient and $\alpha_{\rm n,T} = -(a^2 - r^2)/2rL_{\rm n,T}$ ($L_{\rm n,T}$ is the density or temperature scale length). Comparing the diffusivities for dimensionally similar discharges with different values of ρ_* allows the exponent x_ρ to be determined since the unspecified function F remains constant. In order to keep β, ν_*, and q fixed while varying the magnetic field strength and minor radius, the engineering parameters need to be scaled as $n \propto B^{4/3}a^{-1/3}$, $T \propto B^{2/3}a^{1/3}$, and $I \propto Ba$ while keeping the magnetic geometry fixed. The scaling of the thermal diffusivity for dimensionally similar discharges therefore has the form

$$\chi \propto B^{-(1+2x_\rho)/3} a^{(2-5x_\rho)/6} \quad . \tag{2}$$

The value of the exponent x_ρ could be interpreted as indicating the characteristic wavelength λ of the plasma turbulence responsible for anomalous heat transport: (a) $x_\rho = 1$ would imply $\lambda \sim r_L$, which is called gyro-Bohm-like, (b) $x_\rho = 0$ would imply $\lambda \sim a$, which is called Bohm-like, and (c) $x_\rho = -1$ would imply $\lambda \gg a$, which could arise from having stochastic magnetic fields throughout the plasma. Theoretical work to explain anomalous transport has concentrated on turbulence with characteristic wavelengths of $\lambda \sim r_L$.

Disparate results for the ρ_* scaling of the effective diffusivity (the weighted average of the electron and ion diffusivities) have previously been reported in low (L) mode experiments. In stellarators, dimensionally similar discharge experiments using electron cyclotron heating (ECH) found that the confinement scaling was gyro-Bohm-like[4]; the same conclusion was reached in the DIII–D tokamak[5] for radiofrequency (RF) heating experiments of low density plasmas.[6] However, other tokamak experiments using neutral beam injection (NBI) heating or ion cyclotron heating (ICH) showed that the effective diffusivity followed Bohm-like scaling.[7,8] Experiments with NBI heating of high density plasmas in DIII–D could be fit with either gyro-Bohm-like or Bohm-like models.[9] The radial power flow was dominated by the electron channel (due to direct electron heating) for the experiments which reported gyro-Bohm-like scaling, whereas the radial power flow in the ion channel was significant for the experiments which reported Bohm-like scaling; therefore, one may wonder if the conflicting ρ_* scaling results may be due to different transport scalings for the electrons and ions. A key component in the transport analysis of the dimensionally similar discharge experiments discussed in this paper is the separation of the electron and ion fluids.

The rest of this paper is organized as follows: Section II describes the DIII–D tokamak, auxiliary heating systems, and plasma diagnostics used in these transport experiments. In Section III, the scalings of the electron and ion thermal diffusivities with relative gyroradius for L–mode plasmas are shown, the results of which have been previously reported.[10] In Section IV, dimensionally similar discharges are analyzed for high (H) mode plasmas which match the expected values of β, ν_*, q, and plasma shape for the International Thermonuclear Experimental Reactor[11] (ITER). These

experiments were the first to measure the ρ_* scaling of electron and ion transport in H–mode. The summary and conclusions are given in Section V.

II. EXPERIMENTAL SETUP

For these experiments, plasmas were produced in the DIII–D tokamak with a major radius of $R = 1.7$ m, a minor radius of $a = 0.6$ m, an elongation of $1.7 \leqslant \kappa \leqslant 1.9$, a triangularity of $0.3 \leqslant \delta \leqslant 0.8$, a toroidal magnetic field of $0.95 \leqslant B_T \leqslant 2.0$ T, and a plasma current of $0.5 \leqslant I \leqslant 1.35$ MA. These discharges were all single-null divertor and were fueled by deuterium gas puffing or deuterium NBI. A divertor cryopump was used to control the plasma density for both L–mode and H–mode experiments.

Three forms of auxiliary heating were utilized in these experiments: ECH, fast wave, and NBI. For the ECH frequency of 60 GHz, the electron cyclotron wave was absorbed centrally at 2 T for the fundamental resonance and at 1 T for the second harmonic resonance. The 60 MHz fast wave in the direct electron heating regime was also absorbed near the plasma center since the damping increases with electron temperature. For these experiments, $(0, \pi, 0, \pi)$ phasing of the four-strap fast wave antenna was used to launch a high parallel index of refraction ($|n_\parallel| \approx 9$) which has previously been shown to damp efficiently on electrons for central electron temperatures in excess of 1 keV.[12] Since the hydrogen fraction was measured to be less than 1% during these experiments, second-harmonic hydrogen damping of the fast wave for $B_T = 2$ T was small compared to direct electron damping. Deuterium NBI was used as an alternative to RF heating in some of these transport experiments. The neutral beams heated both electrons and ions.

A number of diagnostics were used to measure the plasma profiles required for a power balance analysis of the radial heat flux. The electron density profile was measured using multi-pulse Thomson scattering[13] along with four CO_2 interferometers. The electron temperature profile was determined by combining data from Thomson scattering and electron cyclotron emission (ECE) measured using a Michelson interferometer and radiometers. The ion temperature profile was found from charge exchange recombination (CER) emission of carbon impurities during neutral beam injection[14]; the ion temperature profiles during RF heating were measured by pulsing the neutral beams for 10 msec to obtain spectroscopic data. The Z_{eff} profile was calculated (using the experimental n_e and T_e profiles) from visible bremsstrahlung light measured

with an array of photodiodes.[15] The radiated power profile was measured by a foil bolometer array.[16] The plasma current profile was determined from an axisymmetric reconstruction of the magnetic equilibrium using the external magnetic measurements, the kinetic profile data, and the magnetic pitch angle measured using the motional Stark effect (MSE).[17,18]

III. TWO-FLUID ANALYSIS OF L–MODE

The radial energy transport can be determined from a steady-state power balance analysis,

$$\nabla \cdot \left(q + \frac{5}{2} \Gamma T \right) = Q \quad , \tag{3}$$

where q is the radial heat flux, Γ is the particle flux, and the heat sources and sinks have been combined into the net power density Q. In general, the heat flux can have both conductive and convective components,

$$q = -n\chi \nabla T + nUT \quad , \tag{4}$$

where U is the convective heat velocity; however, in a power balance analysis these two components of the heat flux cannot be uniquely separated. Therefore, in this paper the heat flux is assumed to be purely conductive; this does not affect the results as long as the ratio of conductive to convective heat flux is independent of ρ_*. If this is not the case, then the measured transport scaling with ρ_* is actually an average of the conductive and convective scalings.

The power balance was computed by the ONETWO transport code, which used the experimental profiles of T_e, T_i, n_e, Z_{eff}, and P_{rad} (the radiated power), along with the magnetic geometry and plasma current profile. The collisional exchange power between electrons and ions was assumed to be classical, and neoclassical resistivity was used in calculating the ohmic power density. The ECH power deposition profile was calculated with the TORAY ray tracing code,[19] while the fast wave power deposition profile was calculated with the CURRAY ray tracing code.[20] The NBI power deposition profile was calculated using a Monte Carlo code. Since all three forms of auxiliary heating were centrally peaked, the transport analysis was not sensitive to possible systematic errors in the modeling of the power deposition profiles.

Three pairs of dimensionally similar L–mode discharges, two with RF heating and one with NBI heating, were analyzed to determine the ρ_* scaling of the electron and ion transport. The engineering parameters for these discharges are shown in Table I. The equilibrium and kinetic stored energies are in good agreement for these discharges. The radial profiles of T_e, T_i, n_e, and Z_{eff} for these three cases are shown in Figs. 1–3. It can be seen that the scalings $T \propto B_T^{2/3}$ and $n \propto B_T^{4/3}$ were obeyed in these figures, thus the nondimensional parameters β, ν_*, α_n, α_T, and T_e/T_i were well matched (see also Ref. 10), as was the normalized power deposition profile outside the central region ($r/a = 0.3$–0.4). The only nondimensional parameters which had a systematic variation for all three pairs of dimensionally similar discharges were Z_{eff} and ρ_* itself.

Table I: Engineering parameters for three pairs of L–mode dimensionally similar discharges

	(a)		(b)		(c)	
	ECH	ECH, FW	ECH	ECH, FW	NBI	NBI
B_T (T)	1.0	2.0	1.0	2.0	1.0	2.0
I_p (MA)	0.5	1.0	0.5	1.0	0.5	1.0
q_{95}	4.8	5.0	5.8	5.9	5.8	5.8
W_{th} (kJ)	42	175	44	179	44	178
P_{tot} (MW)	1.1	2.2	0.6	2.0	0.6	1.9
τ_{th} (msec)	39	81	74	91	74	93

For case (a), the ρ_* scaling of χ_e was found to be gyro-Bohm-like, $x_{\rho e} \approx 1$, as shown in Fig. 4. However, the ρ_* scaling of χ_i was found to be intermediate between Bohm-like and stochastic, $x_{\rho i} \approx -0.5$. This was determined from the ratio of the electron and ion diffusivities for the 2 T and 1 T discharges in conjunction with Eq. (2). Since the scaling of the ion transport coincides with that predicted by the Goldston scaling relation,[21] $\tau \propto IP_{tot}^{-0.5}$ with no n_e or B_T dependence, the scaling $x_\rho = -0.5$ will be referred to as Goldston-like. The error bars in Fig. 4

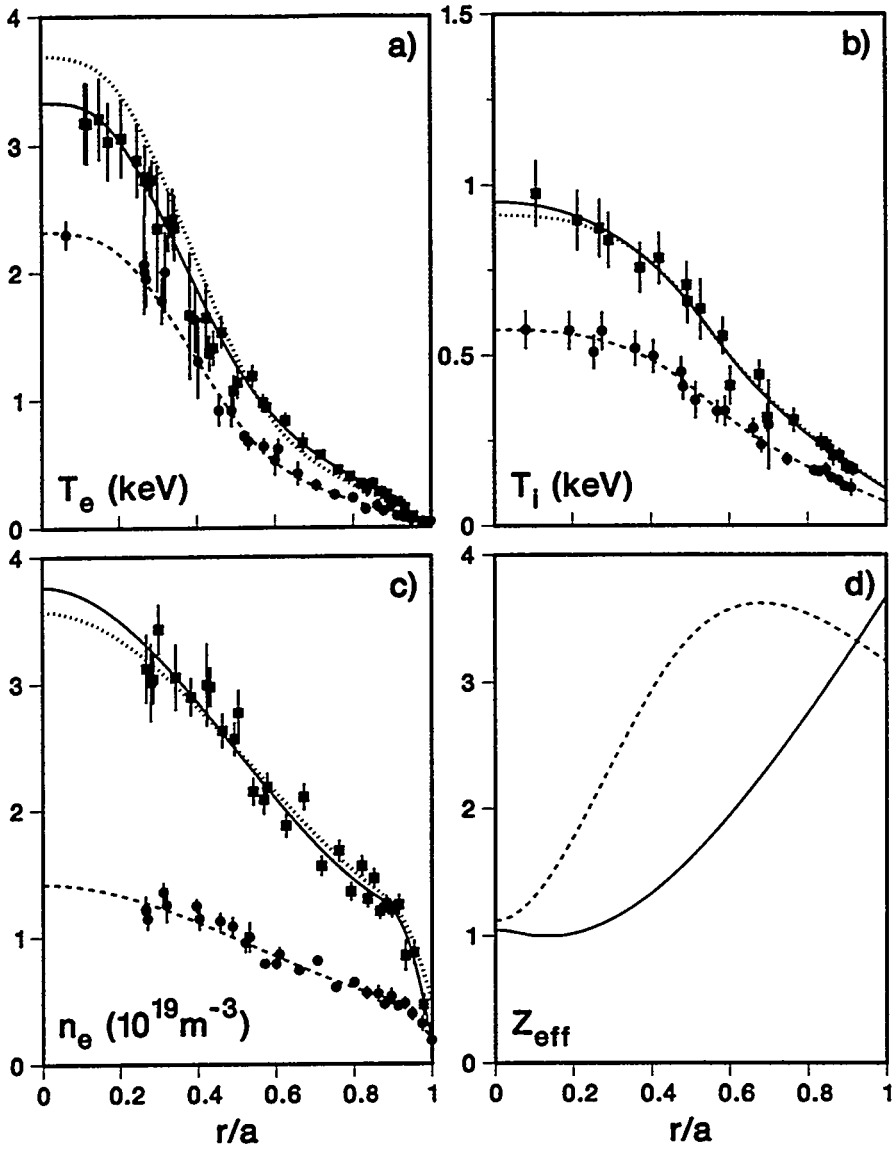

FIG. 1. Radial profiles of a) electron temperature, b) ion temperature, c) electron density, and d) effective ion charge at 2 T (squares and solid lines) and 1 T (circles and dashed lines) for case (a) of Table I. The dotted lines represent the 1 T profiles scaled to 2 T.

are from the combined random errors in the quantities q/nT and $1/L_T$ (systematic errors contribute little uncertainty to the measurement of x_ρ). The error in q/nT was computed by varying the experimental profiles individually by their 1 σ uncertainties and recalculating the power balance; the errors were combined assuming they were uncorrelated. The error in $1/L_T$ was computed by perturbing the spline fit to the

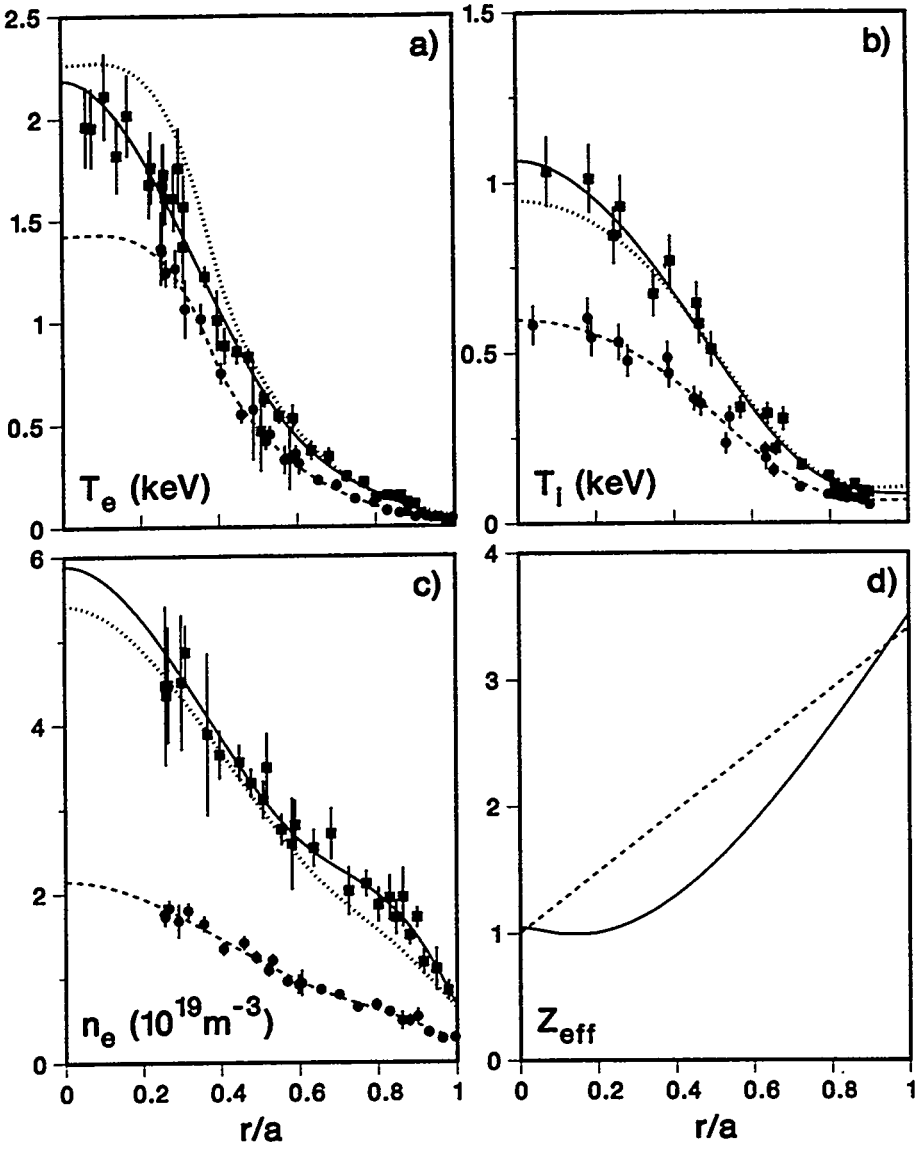

FIG. 2. Radial profiles of a) electron temperature, b) ion temperature, c) electron density, and d) effective ion charge at 2 T (squares and solid lines) and 1 T (circles and dashed lines) for case (b) of Table I. The dotted lines represent the 1 T profiles scaled to 2 T.

profile at the knot locations (one at a time) by its 1 σ uncertainty and recalculating the scale length; the errors were combined by applying standard propagation of errors including the covariance. In Fig. 4, results from the plasma center were not shown due to the effects of sawteeth (the sawtooth mixing radius was located at $r/a = 0.3$),

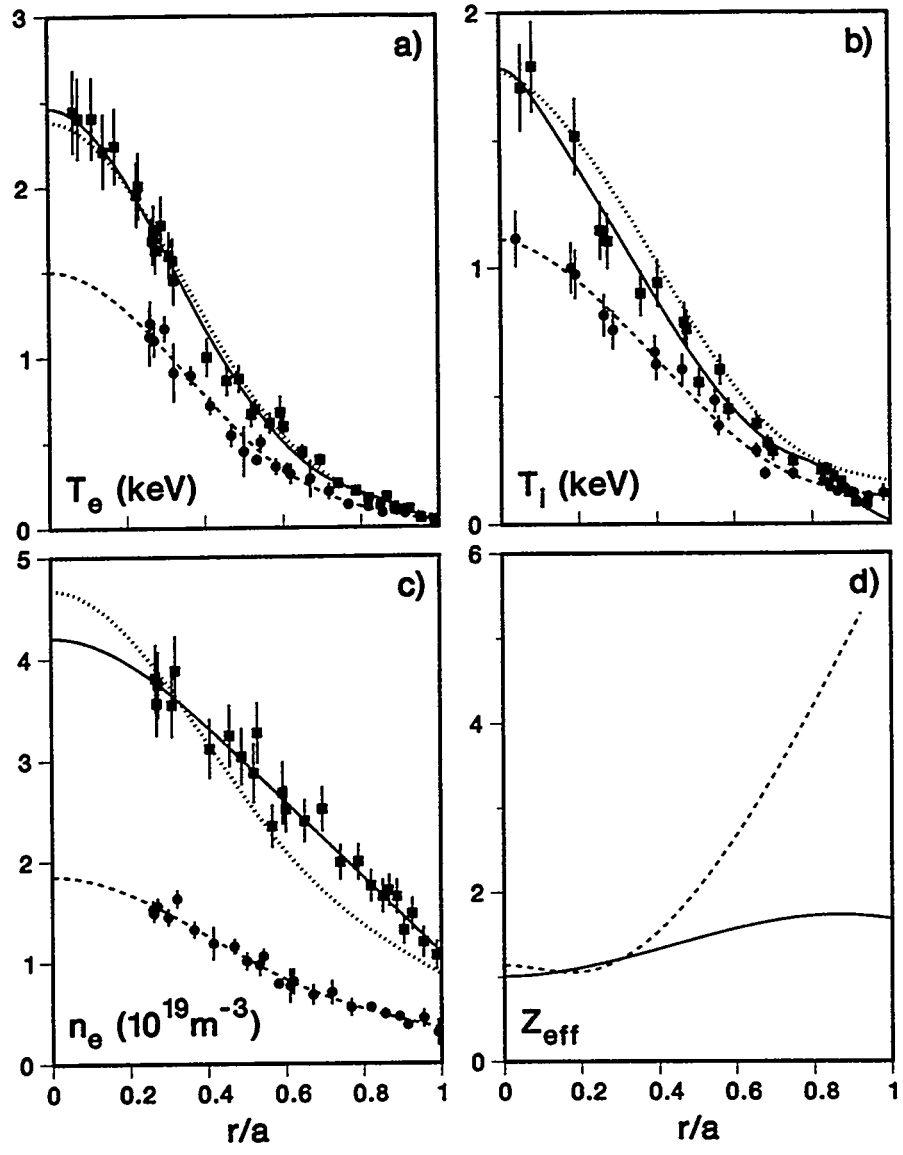

FIG. 3. Radial profiles of a) electron temperature, b) ion temperature, c) electron density, and d) effective ion charge at 2 T (squares and solid lines) and 1 T (circles and dashed lines) for case (c) of Table I. The dotted lines represent the 1 T profiles scaled to 2 T.

while the plasma edge was excluded since the uncertainties in χ_e and χ_i increased rapidly in that area.

Figure 4 also includes the scaling of the effective diffusivity, defined as

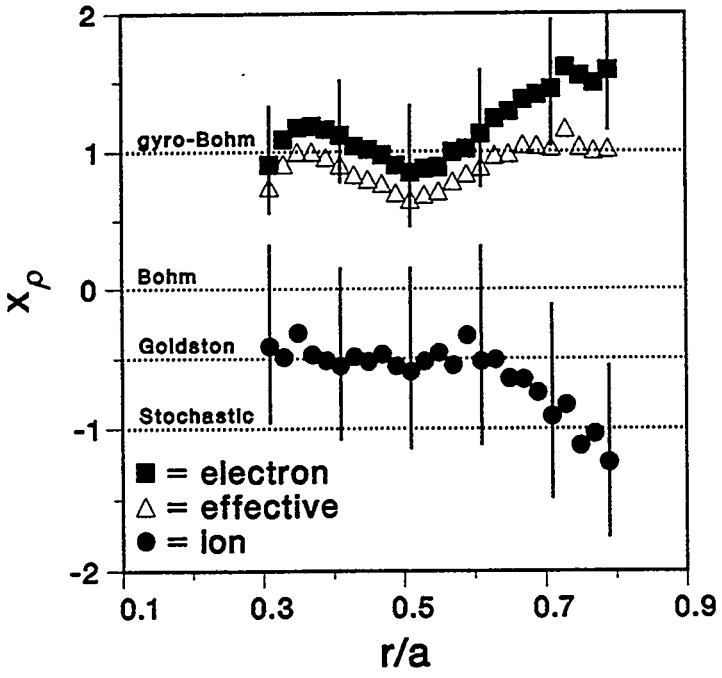

FIG. 4. Measured value of the exponent x_ρ from Eq. (2) for case (a) of Table I.

$$\chi_{\text{eff}} = - \frac{q_e + q_i}{n_e \nabla T_e + n_i \nabla T_i} \quad , \tag{5}$$

which is shown to compare with previous dimensionally similar discharge experiments on tokamaks which analyzed χ_{eff} only.[1,6-9] The effective diffusivity in Fig. 4 has gyro-Bohm-like scaling, as does the global confinement time ($\tau_{\text{th}} \propto B_T^{1.05}$ from Table I). The reason that χ_{eff} and τ_{th} closely follow the ρ_* scaling of the electrons and not the ions was that q_e was three to ten times q_i, due to direct electron heating by the RF waves and weak electron-ion collisional coupling at these low densities.

The dimensionally similar discharges for case (b) were similar to case (a) except that the densities were about 40% higher. This had a significant effect on the global confinement, however, which exhibited Bohm-like scaling, $\tau_{\text{th}} \propto B_T^{0.29}$. The scaling of the effective diffusivity for case (b), shown in Fig. 5, was also Bohm-like. In spite of this, the ρ_* scaling of the electron and ion diffusivities was unchanged between Figs. 4 and 5: χ_e still scaled gyro-Bohm-like while χ_i still scaled Goldston-like. The reason for the different scalings of τ_{th} and χ_{eff} between cases (a) and (b) was that for the

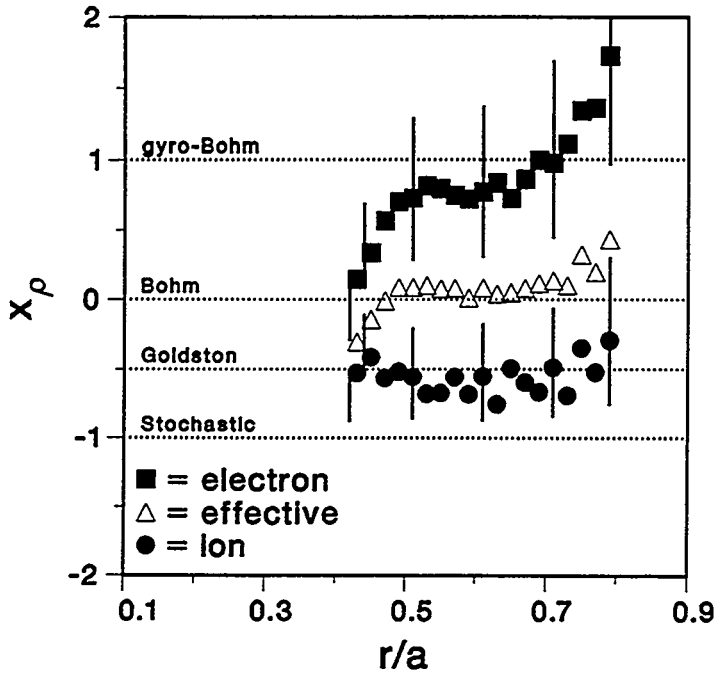

FIG. 5. Measured value of the exponent x_ρ from Eq. (2) for case (b) of Table I.

higher collisionality of case (b), the electron-ion collisional exchange power was much greater, resulting in nearly equal ion and electron heat fluxes. Therefore the scalings of τ_{th} and χ_{eff} with ρ_* was an average of the ion and electron scalings. Since Bohm scaling lies in between gyro-Bohm and Goldston scaling, the scalings of τ_{th} and χ_{eff} appeared to be Bohm-like even though neither species had Bohm-like scaling.

In case (c), NBI heating was utilized instead of RF heating to see if the ρ_* scalings of χ_e and χ_i were dependent upon the method of auxiliary heating. The neutral beam voltage was lowered from 71 kV for the 2 T discharge to 52 kV for the 1 T discharge to help keep T_e/T_i and the normalized power deposition profile constant. As shown in Fig. 6, the electron and ion fluids were found to scale as gyro-Bohm and Goldston, respectively, the same result as obtained with RF heating. Since the electron and ion heat fluxes were both significant for these NBI discharges, χ_{eff} scaled as the average of the electron and ion transport, which was coincidently close to Bohm-like. The thermal confinement time for case (c) also had Bohm-like scaling, $\tau_{th} \propto B_T^{0.33}$. It is especially noteworthy that the ρ_* scaling of ion transport remained unchanged for different methods of auxiliary heating, since for cases (a) and (b) the

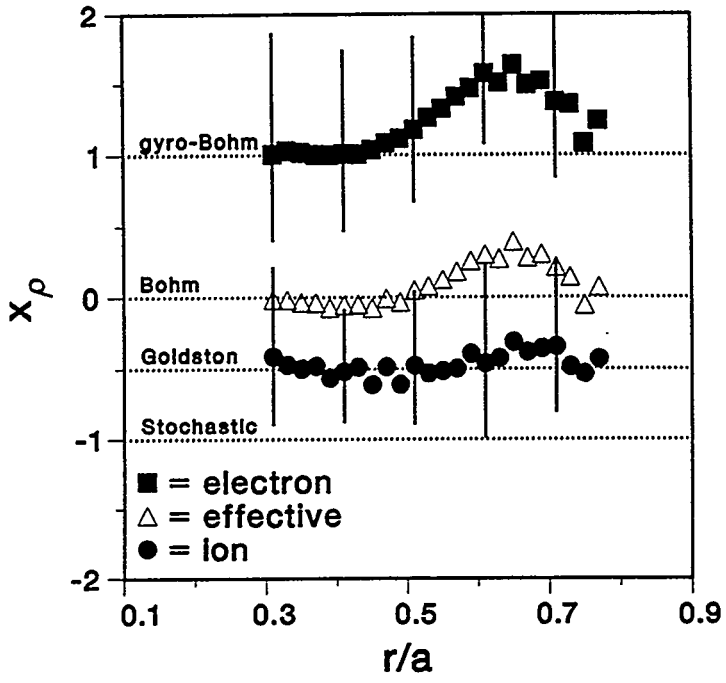

FIG. 6. Measured value of the exponent x_ρ from Eq. (2) for case (c) of Table I.

ion heating was solely due to electron-ion collisional coupling, whereas for case (c) direct beam ion heating was dominant.

Combining the three separate measurements (Figs. 4–6) of the ρ_* scalings for the electron and ion fluids into a final result yields $\chi_e \propto \chi_B \rho_*^{1.1\pm0.3}$ and $\chi_i \propto \chi_B \rho_*^{-0.5\pm0.3}$. Since these scalings were independent of the ratio of electron-to-ion heat flux, they may be considered intrinsic properties of anomalous heat transport. However, since the scalings of χ_{eff} and τ_{th} changed from gyro-Bohm-like when the electrons dominated the total heat flux to Bohm-like when the electron and ion heat fluxes were more equal, the scalings of these parameters are not intrinsic. This demonstrates the problem in using the effective diffusivity or global confinement time to determine transport properties since, in reality, one is measuring the average of possibly different electron and ion scalings.

IV. TWO-FLUID ANALYSIS OF ITER-RELEVANT H–MODE

The scaling of electron and ion diffusivities with relative gyroradius was also measured for H–mode plasmas in DIII–D. The comparison of transport scaling with ρ_* between L–mode and H–mode is of interest since it has been shown that confinement scaling relations derived from multi-machine databases are often more gyro-Bohm-like for H–mode than for L–mode.[22] The purpose of this experiment was to predict the confinement time for H–mode plasmas on ITER and to obtain information on the stability of high β plasmas with the ITER shape. Scaling the measured electron and ion diffusivities in DIII–D along a dimensionally similar path to the ITER magnetic field strength and minor radius allows both the confinement time and the plasma profiles to be predicted for plasmas which are near the conditions required for ignition.

For these experiments, both the ITER plasma shape and the expected ITER plasma parameters (except for ρ_*) needed to be matched in DIII–D. The ITER plasma shape is a low triangularity, single-null divertor with modest elongation; it was possible to match this geometry using $\kappa = 1.68$ and $\delta = 0.36$. Since the ITER major radius is 8.1 m and the minor radius is 3.0 m, DIII–D also has the same inverse aspect ratio as ITER, $\epsilon = 0.37$. Values of the nondimensional plasma parameters for these experiments in DIII–D — $\beta^{\rm th} = 2.3\%$, $\beta_{\rm N}^{\rm th} = 2.1\%/({\rm MA/mT})$, $\nu_{*{\rm i,min}} = 0.01$, and $q_{95} = 3.8$ — were taken from an ITER simulation[23] of an ignited plasma with a H–mode density profile and a fusion power of 1.5 GW.

The engineering parameters for these dimensionally similar discharges in DIII–D with NBI heating are given in Table II. The fast particle contributions have not been included in this table since only the thermal values of the ITER quantities were matched. Since a relatively low density was required to match the ITER collisionality, divertor cryopumping was used in these experiments. The radiative power fraction was 15% for both the 1.9 T and 0.95 T discharges. The radial profiles of six important nondimensional parameters are shown in Fig. 7; the plasma profiles were analyzed after quasi-stationary conditions had been reached in these ELMing H–mode discharges (the profile analysis times were chosen to occur between ELMs). The relative gyroradius was varied by a factor of 1.5 across the plasma while the other

Table II: Engineering parameters for H–mode dimensionally similar discharges on DIII–D and projection to ITER

	DIII–D		ITER
B_T (T)	0.95	1.9	5.7
a (m)	0.62	0.62	3.0
I_p (MA)	0.66	1.33	19.6
$\bar{n}$ (10^{19} m^{-3})	2.8	5.5	14.5
W_{th} (MJ)	0.24	0.91	944
P_{tot} (MW)	3.4	6.1	41
τ_{th} (sec)	0.069	0.148	23.0
H	2.0	2.2	5.3

nondimensional parameters were held nearly constant. The ratio of electron-to-ion temperature was held fixed between the two discharges by changing the neutral beam voltage from 76 kV for the 1.9 T discharge to 53 kV for the 0.95 T discharge. The normalized radial power flows in both the electron and ion channels were also well matched for these two plasmas; the NBI power deposition profile was peaked near the plasma center for both discharges.

An analysis of the heat transport for these dimensionally similar discharges found that both the electron and ion fluids scaled approximately gyro-Bohm-like, $x_{\rho e}, x_{\rho i} \approx 1$, as shown in Fig. 8. This was determined from the ratio of the 0.95 and 1.9 T diffusivities in conjunction with Eq. (2). Although a single value for χ_ρ does not accurately represent the ρ_* scaling due to the radial dependence evident in Fig. 8, gyro-Bohm-like scaling does reflect the average value of χ_ρ. For these H–mode discharges, χ_i was seven times the neoclassical value at $r/a = 0.5$, while χ_e was 30% larger than χ_i at this same radius. The gyroradius scaling of χ_e was the same as for L–mode plasmas discussed in Section III, but the gyroradius scaling of χ_i changed from Goldston-like in L–mode to gyro-Bohm-like in H–mode. Since the electron and ion diffusivities in Fig. 8 had the same ρ_* scaling, the effective diffusivity [defined in Eq. (5)] also had gyro-Bohm-like scaling. From Table II, the thermal confinement

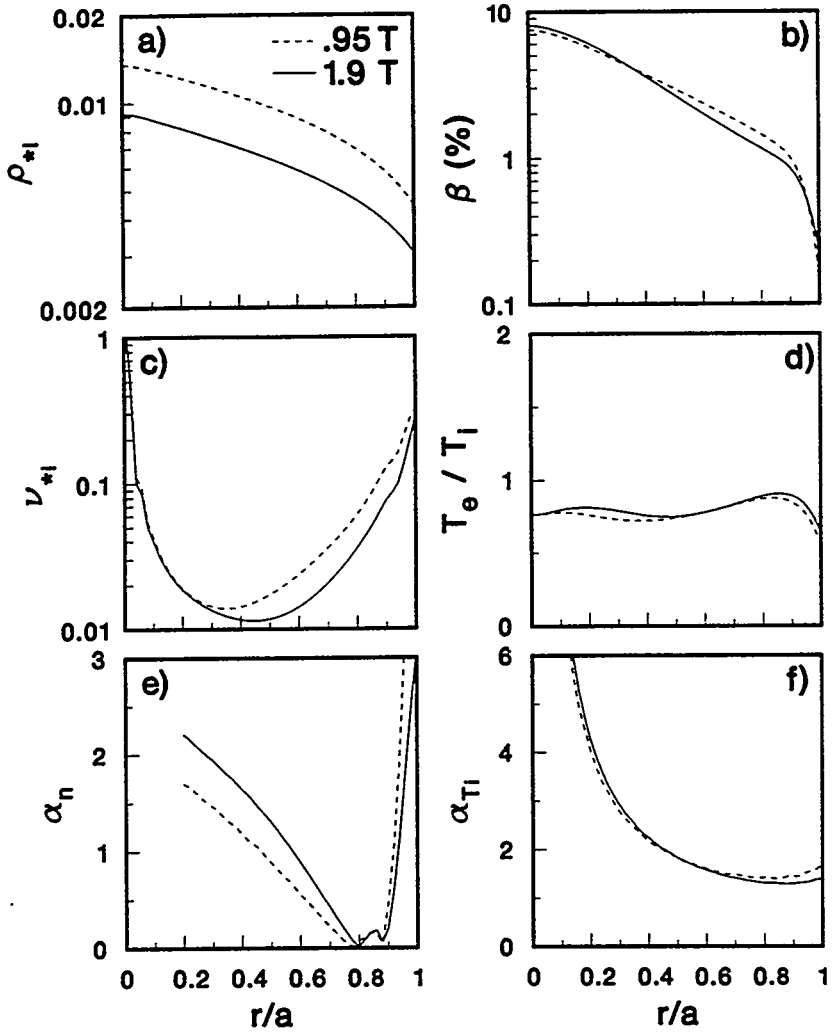

FIG. 7. Radial profiles of a) relative ion gyroradius, b) thermal beta, c) ion collisionality, d) ratio of electron-to-ion temperature, e) nondimensional density scale length, and f) nondimensional ion temperature scale length at 1.9 T (solid lines) and 0.95 T (dashed lines) for H–mode discharges.

time is seen to have gyro-Bohm-like scaling, $\tau_{th} \propto B_T^{1.1}$, in agreement with the scalings of the electron and ion diffusivities.

A relatively low beta limit was observed for these ITER-relevant discharges. For $B_T = 1.9$ T, the highest normalized beta that was achieved was $\beta_N = 2.2$. This beta includes the stored energy of the fast particles. Attempts to further increase beta by injecting additional NBI power resulted in a beta collapse (not a disruption). More

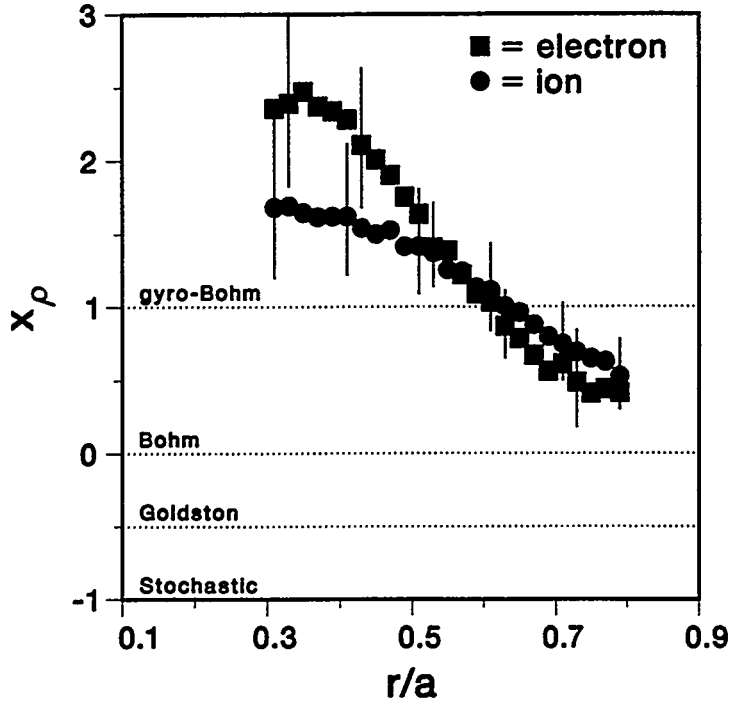

FIG. 8. Measured value of the exponent x_ρ from Eq. (2) for H–mode discharges.

favorable results were obtained at 0.95 T, where a normalized beta of $\beta_N = 2.7$ was achieved. The nature of this beta limit is under study.

Table II also gives the projected parameters for ITER, determined by scaling along a dimensionally similar path from the DIII–D values. Table II shows that the H–factor decreased from 2.2 for the high field discharge to 2.0 for the low field discharge, where the H–factor is defined to be the ratio of the global confinement time (including fast particle contributions) to the ITER–89P scaling relation.[24] The H–factor was not fixed because the ITER–89P scaling relation is nearly Bohm-like[6] whereas the confinement scaling was gyro-Bohm-like, thus along a dimensionally similar path the H–factor must increase with decreasing ρ_*. The thermal confinement time and heating power can be scaled along a dimensionally similar path using the formulas

$$\tau_{th} \propto B^{(1+2x_\rho)/3}\, a^{5(2+x_\rho)/6} \quad , \tag{6}$$

$$P_{tot} \propto B^{(5-2x_\rho)/3}\, a^{(8-5x_\rho)/6} \quad . \tag{7}$$

Thus Table II shows that scaling these DIII–D parameters to ITER results in a predicted H–factor of 5.3, much higher than the assumed H–factor of 2.0 used in the ITER simulation.[23] This high H–factor is a result of the low projected heating power for ITER of 41 MW. However, it is important to note that this predicted heating power does not include any additional heating power that may be required to match the DIII–D boundary conditions for density and temperature projected along a dimensionally similar path to ITER. One important boundary condition is the supposition of H–mode; therefore, if the H–mode power threshold is larger than 41 MW for ITER, then significantly more heating power would be required which would lower the H–factor. For comparison, scaling the L-mode confinement time in DIII–D for the NBI heated plasmas in Table I to the ITER magnetic field strength and size (taking into account the different electron and ion transport scalings) results in a predicted H–factor of only 0.9.

V. SUMMARY AND CONCLUSIONS

Dimensionally similar discharge experiments in the DIII–D tokamak have found that for L–mode plasmas, the electron diffusivity scaled like $\chi_e \propto \chi_B \rho_*^{1.1\pm0.3}$ (gyro-Bohm-like) while the ion diffusivity scaled like $\chi_i \propto \chi_B \rho_*^{-0.5\pm0.3}$ (Goldston-like). These transport scalings were obtained with either central RF heating (ECH and fast wave) or NBI heating. The gyro-Bohm-like scaling of χ_e is the expected result for turbulence generated by small-scale instabilities, but at present there is no clear theoretical explanation for the ρ_* scaling of χ_i. Since χ_e and χ_i have different ρ_* scalings, the effective diffusivity and global confinement time scalings varied from gyro-Bohm-like when the electron channel dominated the total heat flux to Bohm-like when the electron and ion heat fluxes were approximately equal. Thus the different ρ_* scalings of the electron and ion fluids explains the apparently conflicting results reported in the literature for dimensionally similar discharges, where RF heating of low density plasmas in stellarators[4] and tokamaks[6] had gyro-Bohm-like confinement scaling whereas ICH and NBI heating of higher density plasmas in tokamaks[7,8] had Bohm-like confinement scaling.

For H–mode plasmas, both the electron and ion diffusivities were found to have gyro-Bohm-like scaling, $\chi_e, \chi_i \propto \chi_B \rho_*$. The gyro-Bohm-like scaling was also evident in the thermal confinement time for these NBI heated plasmas. Thus the ρ_* scaling of the electron fluid was the same in these L–mode and H–mode experiments, but the ρ_* scaling of the ion fluid changed from Goldston-like in L–mode to gyro-Bohm-like in H–mode. Although the reason for this change in the ion transport scaling is not known, the characteristic difference in the density profiles between L–mode and H–mode (the density scale length is much larger in H–mode) seems a likely candidate.

These H–mode discharges in DIII–D were designed to have the same plasma shape as well as the same beta, collisionality, and safety factor as ITER. Scaling the DIII–D transport results along a dimensionally similar path to ITER results in a predicted H–factor of 5.3. Thus only 41 MW of heating power in ITER would be required to sustain an ignited plasma with 1.5 GW of fusion power; this obviously is not a stable ignition point! However, additional heating power may be needed if the

H–mode power threshold for ITER is larger than 41 MW. The actual confinement time for an ignited deuterium/tritium plasma in ITER will also be affected by the hydrogen-isotope mass scaling of transport, the more equilibrated electron and ion temperatures, and the enhanced bremsstrahlung losses. Even with these qualifications, the observed gyro-Bohm-like scaling of H–mode confinement in DIII–D favors the direction of compact, high-field machines for fusion reactors.

VI. ACKNOWLEDGEMENTS

This is a report of work sponsored by the U.S. Department of Energy under Contract Nos. DE-AC03-89ER51114 and W-7405-ENG-48. The authors would like to thank T.E. Evans, J.R. Ferron, R.J. La Haye, A.W. Leonard, and J.T. Scoville for operating the tokamak during these experiments, M.E. Austin for analyzing the ECE data, A.W. Leonard for analyzing the bolometry data, and F.W. Perkins and D. Boucher for useful discussions on ITER parameters.

VII. REFERENCES

[1]R.E. Waltz, J.C. DeBoo, and M.N. Rosenbluth, Phys. Rev. Lett. **65**, 2390 (1990).

[2]B.B. Kadomtsev, Sov. J. Plasma Phys. **1**, 295 (1975).

[3]J.W. Connor and J.B. Taylor, Nucl. Fusion **17**, 1047 (1977).

[4]U. Stroth, G. Kühner, H. Maassberg, H. Ringler, and W7–AS Team, Phys. Rev. Lett. **70**, 936 (1993).

[5]J.L. Luxon and L.G. Davis, Fusion Technol. **8**, 441 (1985).

[6]C.C. Petty, T.C. Luce, and R.I. Pinsker, in *Radio-Frequency Power in Plasmas: Tenth Topical Conference, Boston, MA 1993* (American Institute of Physics, New York, 1994), p. 165.

[7]F.W. Perkins, C.W. Barnes, D.W. Johnson, S.D. Scott, M.C. Zarnstorff, M.G. Bell, R.E. Bell, C.E. Bush, B. Grek, K.W. Hill, D.K. Mansfield, H. Park, A.T. Ramsey, J. Schivell, B.C. Stratton, and E. Synakowski, Phys. Fluids B **5**, 477 (1993).

[8]J.P. Christiansen, P.M. Stubberfield, J.G. Cordey, C. Gormezano, C.W. Gowers, J. O'Rourke, D. Stork, A. Taroni, and C.D. Challis, Nucl. Fusion **33**, 863 (1993).

[9]R.E. Waltz, J.C. DeBoo, and T.H. Osborne, Nucl. Fusion **32**, 1051 (1992).

[10]C.C. Petty, T.C. Luce, R.I. Pinsker, K.H. Burrell, S.C. Chiu, P. Gohil, R.A. James, and D. Wròblewski, "Gyroradius Scaling of Electron and Ion Transport," submitted to Physical Review Letters.

[11]P-H. Rebut, V. Chuyanov, M. Huguet, R. Parker, and Y. Shimomura, in *Plasma Physics and Controlled Nuclear Fusion Research* (Proc. 15th Int. Conf. Seville, 1994) (International Atomic Energy Agency, Vienna), in press.

[12]C.C. Petty, R.I. Pinsker, M.J. Mayberry, M. Porkolab, F.W. Baity, P.T. Bonoli, S.C. Chiu, J.C.M. de Haas, R.H. Goulding, D.J. Hoffman, T.C. Luce, and R. Prater, Phys. Rev. Lett. **69**, 289 (1992).

[13]T.N. Carlstrom, G.L. Campbell, J.C. DeBoo, R. Evanko, and J. Evans, Rev. Sci. Instrum. **63**, 4901 (1992).

[14]P. Gohil, K.H. Burrell, R.J. Groebner, and R.P. Seraydarian, Rev. Sci. Instrum. **61**, 2949 (1990).

[15]D.P. Schissel, R.E. Stockdale, H. St. John, and W.M. Tang, Phys. Fluids **31**, 3738 (1988).

[16]A.W. Leonard, W.H. Meyer, B. Geer, D.M. Behne, and D.N. Hill, "2-D Tomography with Bolometry in DIII–D," submitted to Review of Scientific Instruments.

[17]L.L. Lao, J.R. Ferron, R.J. Groebner, W. Howl, H. St. John, E.J. Strait, and T.S. Taylor, Nucl. Fusion **30**, 1035 (1990).

[18]D. Wròblewski and L.L. Lao, Rev. Sci. Instrum. **63**, 5140 (1992).

[19]K. Matsuda, IEEE Trans. Plasma Sci. **PS-17**, 6 (1989).

[20]T.K. Mau, S.C. Chiu, and R.W. Harvey, in *Radiofrequency Heating and Current Drive of Fusion Devices 1992* (Proc. 19th Euro. Conf. Brussels) (European Physical Society, Petit-Lancy, 1992), Vol 16E, p. 181.

[21]R.J. Goldston, Plasma Phys. and Contr. Fusion **26**, 87 (1984).

[22]J.P. Christiansen, J.G. Cordey, O.J.W.F. Kardaun, and K. Thomsen, Nucl. Fusion **31**, 2117 (1991).

[23]D. Boucher, private communication (1994).

[24]P.H. Yushmanov, T. Takizuka, K.S. Riedel, O.J.W.F. Kardaun, J.G. Cordey, S.M. Kaye, and D.E. Post, Nucl. Fusion **30**, 1999 (1990).